

Article

# Self-Healing Redox-Active Coatings Based on Ferrocenyl-Containing Polysiloxanes <sup>†</sup>

Artem A. Rashevskii <sup>‡</sup> , Konstantin V. Deriabin <sup>‡</sup> , Elizaveta K. Parshina and Regina M. Islamova <sup>\*</sup> 

Institute of Chemistry, St. Petersburg University, 7/9 Universitetskaya Emb., 199034 St. Petersburg, Russia

\* Correspondence: r.islamova@spbu.ru

<sup>†</sup> In commemoration of the 300th anniversary of St. Petersburg State University's founding.

<sup>‡</sup> These authors contributed equally to this work.

**Abstract:** The known ferrocenyl-containing silicone materials have redox activity and electrical conductivity at the level of antistatic materials, but they are incapable of self-healing due to their irreversible cross-linking, which significantly reduces their application area. The development of novel self-healing ferrocenyl-containing silicone rubbers (FSRs) is a promising area of research that extends the possibilities of their application as protective coatings. In this work, a new method was developed to synthesize FSRs with different ferrocenyl unit content (25 and 50 mol.%) by anionic copolymerization of cyclic octamethylcyclotetrasiloxane (D<sub>4</sub>), cyclic tetraferrocenyl-substituted 1,3,5,7-tetramethyltetrasiloxane (Fc<sub>4</sub>D<sub>4</sub>), and bicyclic cross-linking agent (*bis*-D<sub>4</sub>). The optimal concentrations of the cross-linking agent and ferrocenyl-substituted unit content for FSRs are 5 wt.% and 25 mol.%, respectively. The FSRs exhibit tensile strength and elongation at break up to 0.1 MPa and 215%. The FSRs possess both self-healing at room and/or elevated temperatures (100 °C) and redox activity (Fc/Fc<sup>+</sup> transformations at  $E^0 = 0.43$  V) and conductivity at the antistatic level (*ca.*  $10^{-10}$ – $10^{-11}$  S·cm<sup>-1</sup>). The thermal properties of the FSRs were studied. The proposed approach is relevant for the creation of new functional silicone materials as flexible, self-healing, and antistatic protective coatings.

**Keywords:** self-healing coatings; polysiloxanes; ferrocenyl-containing silicone materials; cross-linking; siloxane equilibrium; antistatic coatings; redox-active coatings



**Citation:** Rashevskii, A.A.; Deriabin, K.V.; Parshina, E.K.; Islamova, R.M. Self-Healing Redox-Active Coatings Based on Ferrocenyl-Containing Polysiloxanes. *Coatings* **2023**, *13*, 1282. <https://doi.org/10.3390/coatings13071282>

Academic Editor: Ni Yang

Received: 30 June 2023

Revised: 18 July 2023

Accepted: 19 July 2023

Published: 21 July 2023



**Copyright:** © 2023 by the authors. Licensee MDPI, Basel, Switzerland. This article is an open access article distributed under the terms and conditions of the Creative Commons Attribution (CC BY) license (<https://creativecommons.org/licenses/by/4.0/>).

## 1. Introduction

Flexible coatings are one of the most important materials from a practical point of view. The main function of such materials is to protect surfaces, equipment, electrical wiring, etc., from external disturbances and weathering [1]. Along with protection, coatings can perform other equally important functions, including antifouling, antibacterial, superhydrophobic, anti-icing, anticorrosive, insulating, and antistatic properties [1–4]. For coatings, the discovery of self-healing opens up new prospects for obtaining durable materials with an extended service life since they can partially or completely recover their initial properties after damage is caused to them [1–5].

Among the most promising polymers for the production of protective coatings are silicones (polysiloxanes), since they exhibit high flexibility, stretchability, bioinertness, hydrophobicity, high thermal and frost resistance, high gas permeability, and stability to UV and ozone [6–8]. The silicones also possess one of the lowest glass transition temperatures (–123 °C) as distinguished from other polymers [6–10], making them potential for applications at very low temperatures and extreme weather conditions. The silicone materials have good adhesion to a wide range of substrates while maintaining substantial weather and biofouling resistance.

Various self-healing silicone coatings are known to date, such as antifouling and antibacterial [11–16], superhydrophobic [17–20], anti-icing [21], anticorrosive [15,22–27], insulating [28–30], antistatic, and coatings to prevent electrical breakdown [30–33]. Antistatic

self-healing coatings for electrical engineering, electronics, and optoelectronics are also in great demand [1–5,34,35]. Most of the works are devoted to the creation of antistatic materials based on polymer composites [1–4,34–36] by using conductive fillers (graphite [37,38], carbon nanotubes and nanofibers [39–46], graphene [39,40,47,48], metals [38–40,49], metal oxides [45,46],  $\pi$ -conjugated polymers [40,50,51], etc.) to transform a silicone dielectric into a semiconductor (conductivity of ca.  $10^2$ – $10^{-10}$  S·m<sup>-1</sup> [51,52]). Along with huge benefits, composites exhibit their drawbacks, including leaching of fillers under the action of solvents (by rain, soaking with alcohols, etc.) and promotion of the irregular filler distribution in a silicone matrix, causing stratification of a composite material [36,53]. Some fillers (graphite, carbon black, silicon carbide, etc.) make a polymer composite toxic and decrease its tensile properties [36]. Therefore, to impart antistatic and redox-active properties, the most effective approach is to functionalize the polysiloxane backbone with redox-active substituents [9,54–57]. The ferrocenyl group is chemically sustainable in the air at room temperature (RT, 25 °C), with an easy and stable one-electron redox transition, making it one of the most suitable side substituents to obtain antistatic protective coatings [58,59].

Previously, we had already obtained ferrocenyl-containing silicone materials that did not have self-healing ability [9]. Thus, antistatic coatings [54], redox-active layers for flexible optoelectronic devices [55], prototypes of neuronal implants [56], and stretchable electrochromic materials [57] were prepared on their basis. The discovery of siloxane equilibrium [60–65] is the key to synthesizing self-healing silicone rubbers (by ring-opening anionic polymerization, ROAP), which provides new opportunities for the creation of multifunctional materials exhibiting a triple function: (i) flexibility and stretchability, (ii) antistatic properties and redox activity, and (iii) a self-healing ability.

Hence, the general aim of the current study is to develop a method for obtaining protective ferrocenyl-containing silicone coatings with antistatic and redox properties due, on the one hand, to modification of the main polysiloxane chain by ferrocenyl groups and, on the other hand, to self-healing properties by introducing dynamic cross-links via the siloxane equilibrium mechanism. To achieve this goal, it is necessary to solve the following tasks: (i) synthesis of a new, previously unused bicyclic oligosiloxane cross-linking agent (*bis*-D<sub>4</sub>) containing a Si–O–Si linker and cyclic tetraferrocenyl-substituted 1,3,5,7-tetramethyltetrasiloxane (Fc<sub>4</sub>D<sub>4</sub>); (ii) preparation of self-healing ferrocenyl-containing silicone rubbers (FSRs) by a cross-linking reaction between cyclic octamethylcyclotetrasiloxane (D<sub>4</sub>), Fc<sub>4</sub>D<sub>4</sub>, and the cross-linking agent (*bis*-D<sub>4</sub>); (iii) selection of the optimal cross-linking degree and ferrocene content; and (vi) characterization of the obtained FSRs: determination of swelling parameters, evaluation of tensile and self-healing properties, redox activity, electrical conductivity, and thermal properties.

## 2. Materials and Methods

### 2.1. Materials

Octamethylcyclotetrasiloxane (D<sub>4</sub>, 98%), 1,3,5,7-tetramethylcyclotetrasiloxane (H<sub>4</sub>D<sub>4</sub>, 98%), 1,1,3,3-tetramethyl-1,3-divinyl-disiloxane (98%), 1,3,3,5,5,7,7-heptamethylcyclotetrasiloxane (HD<sub>4</sub>, 95%), and platinum (0)-1,3-divinyl-1,1,3,3-tetramethyldisiloxane complex 0.1 M solution in xylene were purchased from Abcr GmbH (Karlsruhe, Germany) and utilized as received. Vinylferrocene was synthesized from ferrocene (98%, Shanghai Macklin Biochemical Co., Shanghai, China) according to the known three-step procedures [54,66]. Previously described substances were analyzed by nuclear magnetic resonance (NMR) spectroscopy before being used. CH<sub>2</sub>Cl<sub>2</sub> (99%), CHCl<sub>3</sub> (99%), hexane (99%), acetone (99%), and EtOH (95%) were purchased from Vecton (St. Petersburg, Russia) and used without additional purification. Toluene (99%, Vecton, St. Petersburg, Russia) and CH<sub>3</sub>CN (99%, Vecton, St. Petersburg, Russia) were freshly distilled over Na/benzophenone and P<sub>4</sub>O<sub>10</sub>, respectively, under argon before usage. Tetramethylammonium (3-aminopropyl)dimethylsilanoate (APDMST) was synthesized from 1,3-bis(3-aminopropyl)tetramethyldisiloxane (97%) and 25 wt.% tetramethylammonium hydroxide solution in MeOH (TMAH, Abcr GmbH, Karl-

sruhe, Germany) according to the known procedure [67]. H<sub>2</sub>O was distilled prior to use. LiClO<sub>4</sub> (99%, Merck, St. Louis, MO, USA) was recrystallized from H<sub>2</sub>O.

## 2.2. Methods

### 2.2.1. Spectroscopic Characterization

The NMR spectra were obtained using a Bruker Avance III 400 spectrometer (Bruker, Santa Barbara, CA, USA) in CDCl<sub>3</sub> at RT operating at 400 MHz for <sup>1</sup>H, 100 MHz for <sup>13</sup>C, and 80 MHz for <sup>29</sup>Si NMR, respectively. Chemical shifts of signals are shown in δ-values [ppm] referenced to the residual signals of CHCl<sub>3</sub>: δ 7.26 (<sup>1</sup>H) and 77.2 (<sup>13</sup>C). The following abbreviations are utilized to designate multiplicities of signals: s = singlet, q = quartet, m = multiplet, and br = broad.

The solid-state NMR (SSNMR) spectra of silicone rubbers as prepared powders were recorded on a Bruker AVANCE III 400-MHz WB spectrometer (Bruker, Santa Barbara, CA, USA) operating at 400.23 MHz for <sup>1</sup>H (16 scans), 100.64 MHz for <sup>13</sup>C (2000 scans), and 79.51 MHz for <sup>29</sup>Si (2000 scans) under magic-angle spinning conditions with spin rates of ca. 12,500 Hz. <sup>13</sup>C and <sup>29</sup>Si SSNMR spectra were obtained using cross-polarization (typically with a contact time of 2 ms and a recycle delay of 2 s) with <sup>1</sup>H decoupling. Chemical shifts of signals are shown in δ-values [ppm] referenced with respect to pure Si(CH<sub>3</sub>)<sub>4</sub>.

High-resolution mass spectra (HRMS) were recorded in a positive ion mode (*m/z* = 50–3000) using a Bruker Maxis HRMS-ESI-qTOF spectrometer (Bruker, Santa Barbara, CA, USA) equipped with an electrospray ionization source. The analyzed compounds were dissolved in neat MeOH prior to the HRMS measurements. The most intensive peak in the isotopic pattern is noted.

Metal content was established by using energy-dispersive X-Ray (EDX) analysis. A ferrocenyl-containing silicone rubber with a mass of ca. 100 mg was solubilized in a HF/HNO<sub>3</sub> mixture (1:4, *V/V*) in sealed polytetrafluoroethylene (PTFE) tubes with an Ethos ONE microwave digestion system (Milestone Srl., Sorisole, Italy). The obtained solution was centrifuged at 3000 rpm for 5 min and then poured into a polypropylene film cup. Afterwards, an EDX analysis of it was conducted by a Shimadzu EDX-800P spectrometer (Shimadzu, Kyoto, Japan). The iron concentration was estimated on a 6.40 KeV FeK $\alpha$  line with signal accumulation for 100 s of live time. Before the analysis, anhydrous FeCl<sub>3</sub> (Abr GmbH, Karlsruhe, Germany) was dissolved in HF/HNO<sub>3</sub> (1:4, *V/V*) in order to construct a calibration curve for the required concentration range, and a blank HF/HNO<sub>3</sub> mixture (1:4, *V/V*) was analyzed for the baseline correction. The iron content in polymer samples was calculated with the following Equation (1):

$$\omega_{Fe}, \% = \frac{C \cdot V}{1,000,000 \cdot m_{sample}} \times 100\%, \quad (1)$$

where *C*—measured Fe<sup>3+</sup> content in a solution, mg·L<sup>-1</sup>; *V*—volume of the solution (*V* = 5 mL); and *m<sub>sample</sub>*—mass of the polymer sample.

### 2.2.2. Swelling Properties

**Polymer density.** The polymer density was determined via the pycnometric method using distilled H<sub>2</sub>O [57]. The density of a silicone rubber ( $\rho_p$ ) was calculated by Equation (2):

$$\rho_p = \frac{m}{m_1 - m_2 + m} \quad (2)$$

where  $\rho_0 = 0.997 \text{ g} \cdot \text{mL}^{-1}$ —the density of distilled H<sub>2</sub>O; *m*<sub>1</sub>—the mass of the pycnometer filled with distilled H<sub>2</sub>O up to the mark; *m*—the total mass of solid polymer samples (approximately 10 pellets); and *m*<sub>2</sub>—the mass of the pycnometer with H<sub>2</sub>O and solid polymer samples (in this case, excess H<sub>2</sub>O was removed using filter paper up to the mark).

**Cross-linking degree.** Swelling measurements were conducted to estimate the cross-linking degree of silicone rubbers [57]. Toluene (125 mL) was added to a flask attached

to a Soxhlet extractor and reflux condenser, and the cylindrical polymer samples with a diameter of 10 mm and a thickness of 1–2 mm (at least 4 samples for each series of silicone rubbers) were put into the thimble inside the extractor. The swelling process was conducted by toluene refluxing for 2 h. Afterwards, the silicone samples were taken out of the Soxhlet extractor and instantly weighed to calculate the swelling percentage ( $s$ ) by using Equation (3). The silicone samples were then dried at RT overnight, then at 100 °C under vacuum for 2 h and weighed again. The soluble fraction ( $\omega_{sol}$ ) and gel fraction ( $v$ ) were calculated using Equations (4) and (5):

$$s = \frac{m_s}{m_{unex}} \times 100\%, \quad (3)$$

$$\omega_{sol} = \frac{m_{unex} - m_{ex}}{m_{unex}} \times 100\%, \quad (4)$$

$$v = \left[ 1 + \frac{m_s - m_{ex}}{m_{ex}} \times \frac{\rho_p}{\rho_s} \right]^{-1}, \quad (5)$$

where  $m_{unex}$ —the mass of an initial dry silicone sample;  $m_s$ —the mass of the swelled silicone sample;  $m_{ex}$ —the mass of the dried silicone sample after swelling; and  $\rho_s$  and  $\rho_p$  are the toluene (0.87 g·mL<sup>-1</sup>) and polymer densities, respectively.

The cross-linking degree ( $\rho_{cross}$ ) and average molecular weight of segments between cross-links ( $M_c$ ) were calculated using Equations (6) and (7) [68]:

$$\rho_{cross} = -\frac{1}{V_s} \times \left[ \frac{\ln(1-v) + v + \chi v^2}{v^{\frac{1}{3}} - \frac{v}{2}} \right] \quad (6)$$

$$M_c = \frac{\rho_p}{\rho_{cross}} \quad (7)$$

where  $V_s = 106.3 \text{ mL} \cdot \text{mol}^{-1}$ —the toluene molar volume;  $\chi = 0.465$ —the Flory–Huggins parameter for polymer–solvent interaction (polydimethylsiloxane–toluene); and  $\rho_s = 0.87 \text{ g} \cdot \text{mL}^{-1}$ —the toluene density.

### 2.2.3. Mechanical Tensile and Self-Healing Tests

Mechanical stress–strain tests were conducted on a Shimadzu EZ-L-5kN universal testing machine at RT and constant stretching rates of 40 mm·min<sup>-1</sup>. The experiments were carried out at least 5 times for each series of silicone samples cut using the ISO 37 Type 3 standard. The elongation at break ( $\varepsilon$ ) was calculated by the following Equation (8):

$$\varepsilon = \frac{l_{break} - l}{l} \times 100\% \quad (8)$$

where  $l_{break}$ —the length of the measured working area of a silicone sample at the moment of rupture; and  $l$ —the initial length of the determined working area of a silicone sample.

The hysteresis (residual elongation,  $\varepsilon_{residual}$ ) was defined as irreversible residual deformation, expressed in percent after a tension test of a polymer sample.

The self-healing efficiency ( $\eta$ ) of silicone rubbers was estimated by tensile tests according to the published method [69–71]. A crosscut (similar to a “natural” through-the-thickness crack) was carefully made in the working area of a silicone strip using a thin razor blade. Afterwards, self-healing of the silicone strips was instantly conducted in aerobic conditions at RT or by heating up to 100 °C in a thermostatic chamber for different time intervals (from 5 min to 24 h). Following that, tension tests of original and healed silicone strips were carried out at RT to determine their  $\eta$  parameter via Equation (9):

$$\eta = \frac{\sigma_{healed}}{\sigma} \times 100\% \quad (9)$$

where  $\sigma_{healed}$  and  $\sigma$ —the tensile strengths of healed and original silicone strips.

#### 2.2.4. Cyclic Voltammetry

Cyclic voltammetry (CV) with different scan rates was carried out on an AutoLab PG-STAT30 (Metrohm, Herisau, Switzerland) potentiostat using a classical glass three-electrode electrochemical cell, which consisted of a working electrode (glassy carbon (GC) coated with a redox-active polymer), a counter electrode (auxiliary platinum electrode, 15.0 cm<sup>2</sup>), and a reference electrode (Ag | AgCl, NaCl<sub>sat</sub>, BASi<sup>®</sup> MF-2052) (Bioanalytical Systems, West Lafayette, IN, USA). The cell was connected to the potentiostat via terminals. The working GC electrode (0.07 cm<sup>2</sup>, BASi<sup>®</sup> MF-2012) (Bioanalytical Systems, West Lafayette, IN, USA) was polished using aqueous suspensions of aluminum oxide and diamond, rinsed with distilled H<sub>2</sub>O, acetone, and EtOH, and dried in the air. The GC electrode was used for CV measurements, whereas indium-tin oxide (ITO) glass was used as the working electrode for the demonstration of the electrochromic (EC) property of a redox-active polymer. The uncured viscous mixtures of monomers D<sub>4</sub>, Fc<sub>4</sub>D<sub>4</sub>, and bis-D<sub>4</sub> (pre-polymerized using APDMST as an initiator at 100 °C for 1 h) were previously deposited on the working electrode via drop-casting (in the case of the GC electrode) and spin-coating methods (in the case of the ITO electrode using a EZ4 spin coater, time of 60 s, rotation speed of 10,000 rpm, and acceleration of 5000 rpm·s<sup>-1</sup>), followed by cross-linking of polymers on the electrode surface at 90 °C for 2 h. A 0.1 M solution of LiClO<sub>4</sub> in a H<sub>2</sub>O–CH<sub>3</sub>CN mixture (4:1, V/V) was utilized as a supporting electrolyte. Prior to the electrochemical measurements, a gentle stream of dry argon was blown through the solution to prevent the ingress of oxygen from the air. In order to reach the stable CV shape, the polymer films were cycled in the monomer-free electrolyte (a 0.1 M solution of LiClO<sub>4</sub> in a 4:1 H<sub>2</sub>O–CH<sub>3</sub>CN mixture), ranging from –0.3 V to +1.1 V at the potential scan rate of 20 mV·s<sup>-1</sup> for 5–6 cycles. The thin polymer films prepared on the GC electrodes were tested by CV with different potential sweep rates (10, 20, 50, 100, 200, 500, and 1000 mV s<sup>-1</sup>) ranging from 0 to 0.8 V vs. Ag | AgCl using the IR compensation feature (approximately 50 Ω).

#### 2.2.5. Broadband Impedance Spectroscopy

The specific electrical conductivity of silicone rubbers was estimated on a Novocontrol Alpha Broadband Dielectric Spectrometer (Novocontrol Technologies GmbH & Co. KG, Montabaur, Germany) at RT, as reported in the references [54,56,57,69,70]. A ZGS-shielded sample cell kept a round silicone film with a diameter of 2 cm and a thickness of 0.4–0.6 mm between two gold-plated brass electrodes. In order to provide full surface electric contact, the analyzed silicone film was coated with 10 nm of carbon film by thermal sputtering with the use of a Q150 TES coater (Quorum Technologies, Laughton, UK). The temperature of the system was controlled by evaporated liquid N<sub>2</sub> flowing through gas heaters. The polymer films were held for at least 300 s at RT to reach thermal equilibrium before the estimation of conductivity. The measurement sequence included a frequency sweep (0.1–1000.0 Hz; 10 points per decade) with a 30 mV signal amplitude. At least 5 tests were carried out per frequency step, and then median-specific resistance averaging was performed.

#### 2.2.6. Thermal Analysis Methods

Thermogravimetry (TG) of the silicone rubbers was carried out on a NETZSCH TG 209F1 Libra TGA209F1D0024 analyzer (Erich Netzsch GmbH & Co., Selb, Germany) at a heating rate of 10 °C·min<sup>-1</sup> from 30 to 800 °C in an aerial atmosphere.

Differential scanning calorimetry (DSC) of silicone samples was carried out on the NETZSCH DSC 204F1 Phoenix instrument (Erich Netzsch GmbH & Co., Naperville, IL, USA) to estimate the glass transition temperature ( $T_g$ ), crystallization, and melting points. Before DSC experiments, the silicone rubbers had been cooled from 0 to –140 °C. The DSC conditions were the following: heating from –140 to 0 °C at a heating rate of 10 °C·min<sup>-1</sup>. The DSC measurements were performed at least twice for each silicone sample.

### 2.3. Synthesis of 1,3-Bis(2-(2,4,4,6,6,8,8-heptamethyl-1,3,5,7,2,4,6,8-tetraoxatetrasiloxan-2-yl)ethyl)-1,1,3,3-tetramethyldisiloxane (Bis-D<sub>4</sub>)

A solution of Karstedt's catalyst in xylene (0.1 M, 100  $\mu$ L) was diluted with freshly distilled toluene (5 mL) in a flask under argon and purged with argon for 5 min. Afterwards, 1,1,3,3-tetramethyl-1,3-divinyldisiloxane (1.00 g, 5.36 mmol) was added to the resulting solution. To activate the catalyst, the obtained solution was stirred at RT for approximately 2 h, and then a gentle stream of argon passed through it for 1 min. The pre-prepared solution of HD<sub>4</sub> (2.88 g, 10.19 mmol) in freshly distilled toluene (5 mL) was added by drops to the reaction mixture for 1 h under argon, and then the reaction mixture was sealed and stirred at RT overnight. The resulting solution was filtered through a silica gel layer (1 cm) to remove the formed platinum black, and the solvent was then evaporated under reduced pressure. Yield: 3.48 g (86%); viscous, colorless oil. <sup>1</sup>H NMR (CDCl<sub>3</sub>,  $\delta$ ): 0.01–0.14 (br m, 54H, CH<sub>3</sub>Si), 0.46 (m, 6.3H, –SiCH<sub>2</sub>CH<sub>2</sub>Si–), 0.94 (q, 0.2H, –SiCH(CH<sub>3</sub>)Si–), and 1.06 (m, 0.6H, –SiCH(CH<sub>3</sub>)Si–). <sup>13</sup>C NMR (CDCl<sub>3</sub>,  $\delta$ ): –1.6 (SiD<sub>4</sub>(CH<sub>3</sub>–), –0.4 (–Si(CH<sub>3</sub>)<sub>2</sub>OSi(CH<sub>3</sub>)<sub>2</sub>–), 0.8 (SiD<sub>4</sub>), 7.7 (SiD<sub>4</sub>CH(CH<sub>3</sub>)Si(CH<sub>3</sub>)<sub>2</sub>O–), 8.5 (SiD<sub>4</sub>CH<sub>2</sub>CH<sub>2</sub>Si(CH<sub>3</sub>)<sub>2</sub>O–), 9.4 (SiD<sub>4</sub>CH<sub>2</sub>CH<sub>2</sub>Si(CH<sub>3</sub>)<sub>2</sub>O–), and 11.5 (SiD<sub>4</sub>CH(CH<sub>3</sub>)Si(CH<sub>3</sub>)<sub>2</sub>O–). <sup>29</sup>Si NMR (CDCl<sub>3</sub>,  $\delta$ ): –20.0 (SiD<sub>4</sub>), –19.7 (*ipso*-SiD<sub>4</sub>CH<sub>2</sub>CH<sub>2</sub>–), –19.3 (SiD<sub>4</sub>), –19.2 (*ipso*-SiD<sub>4</sub>CH(CH<sub>3</sub>)–), 7.5 (–OSi(CH<sub>3</sub>)<sub>2</sub>CH(CH<sub>3</sub>)–), 8.0 (–CH(CH<sub>3</sub>)Si(CH<sub>3</sub>)<sub>2</sub>OSi(CH<sub>3</sub>)<sub>2</sub>CH<sub>2</sub>CH<sub>2</sub>–), and 8.2 (–OSi(CH<sub>3</sub>)<sub>2</sub>CH<sub>2</sub>CH<sub>2</sub>–). HRMS<sup>+</sup>: calculated for C<sub>22</sub>H<sub>62</sub>O<sub>9</sub>Si<sub>10</sub>Na<sup>+</sup> 773.1984, found *m/z* 773.1981 [M + Na]<sup>+</sup>.

### 2.4. Synthesis of 1,3,5,7-Tetraferrocenyl-1,3,5,7-tetramethylcyclotetrasiloxane (Fc<sub>4</sub>D<sub>4</sub>)

The synthesis of Fc<sub>4</sub>D<sub>4</sub> was carried out via a previously published method [72], but with some modifications. A solution of Karstedt's catalyst in xylene (0.1 M, 100  $\mu$ L) was diluted with freshly distilled toluene (5 mL) in a round-bottom flask under an argon atmosphere and purged with argon for 5 min. Afterwards, vinylferrocene (1.50 g, 7.07 mmol) was added to the resulting solution. To activate the catalyst, the obtained red solution was stirred at RT for approximately 2 h, and then a gentle stream of argon passed through it for 1 min. A pre-prepared solution of H<sub>4</sub>D<sub>4</sub> (0.41 g, 1.70 mmol) in freshly distilled toluene (5 mL) was added by drops to the reaction mixture for 1 h under argon, and then the reaction mixture was sealed and stirred at RT overnight. During the reaction, the color of the solution changed to a dark brown. The obtained mixture was then evaporated under reduced pressure, thereby obtaining a brown oil. The target product was purified using silica gel column chromatography (CH<sub>2</sub>Cl<sub>2</sub>/hexane, 1:3 (V/V), R<sub>f</sub> = 0.65). Yield: 1.62 g (83%); viscous brown oil. <sup>1</sup>H NMR (CDCl<sub>3</sub>,  $\delta$ ): 0.00–0.25 (m, 12H, CH<sub>3</sub>Si), 0.76–0.98 (m, 7.3H,  $\equiv$ SiCH<sub>2</sub>CH<sub>2</sub>Fc), 1.43 (m, 1.8H,  $\equiv$ SiCH(CH<sub>3</sub>)Fc), 1.85 (m, 0.6H,  $\equiv$ SiCH(CH<sub>3</sub>)Fc), 2.31–2.51 (m, 7.2H,  $\equiv$ SiCH<sub>2</sub>CH<sub>2</sub>Fc), and 4.03–4.25 (br m, 36H, Fc). <sup>13</sup>C NMR (CDCl<sub>3</sub>,  $\delta$ ): –0.4 (CH<sub>3</sub>Si), 18.5 ( $\equiv$ SiCH<sub>2</sub>CH<sub>2</sub>Fc), 22.8 ( $\equiv$ SiCH<sub>2</sub>CH<sub>2</sub>Fc), 67.1 (3,4-C<sub>5</sub>H<sub>4</sub>CH<sub>2</sub>CH<sub>2</sub>–), 67.6 (2,5-C<sub>5</sub>H<sub>4</sub>CH<sub>2</sub>CH<sub>2</sub>–), 68.4 (Cp), and 92.0 (*ipso*-C<sub>5</sub>H<sub>4</sub>CH<sub>2</sub>CH<sub>2</sub>–). <sup>29</sup>Si NMR (CDCl<sub>3</sub>,  $\delta$ ): –20.4 ( $\equiv$ SiCH(CH<sub>3</sub>)Fc) and –20.2 ( $\equiv$ SiCH<sub>2</sub>CH<sub>2</sub>Fc). HRMS<sup>+</sup>: calculated for C<sub>52</sub>H<sub>64</sub>Fe<sub>4</sub>O<sub>4</sub>Si<sub>4</sub> 1088.1280, found *m/z* 1088.1295 [M]<sup>+</sup>.

### 2.5. Preparation of Model Self-Healing Silicone Rubbers

Model self-healing silicon rubbers (MSRs) were synthesized with different amounts of *bis*-D<sub>4</sub>: 0.5 (PDMS*bis*-D<sub>4</sub>-0.5), 0.75 (PDMS*bis*-D<sub>4</sub>-0.75), and 1.0 wt.% (PDMS*bis*-D<sub>4</sub>-1.0), respectively. The bulk polymerization with further cross-linking was conducted by mixing *bis*-D<sub>4</sub> (25.0 mg, 0.03 mmol for PDMS*bis*-D<sub>4</sub>-0.5; 37.5 mg, 0.05 mmol for PDMS*bis*-D<sub>4</sub>-0.75; and 50.0 mg, 0.07 mmol for PDMS*bis*-D<sub>4</sub>-1.0) with D<sub>4</sub> (5.00 g, 16.86 mmol) and APDMST (3.50 mg, 0.02 mmol) in a round-bottom flask under argon at 100 °C. Afterwards, the reaction mixture was sealed and stirred at 100 °C for 10–15 min. The formed viscous gel was poured into a PTFE mold with a surface area of 160 mm length  $\times$  40 mm width and then cross-linked at 100 °C for 24 h. The obtained polymer films with a thickness of  $\approx$ 1 mm were peeled off the PTFE mold and cut out to obtain shapes according to the requirements of further experiments.

### 2.6. Preparation of Self-Healing Ferrocenyl-Containing Silicone Rubbers

Self-healing ferrocenyl-containing silicon rubbers (FSRs) were synthesized with different contents of ferrocenyl-containing units: 25 (FSR25) and 50 mol% (FSR50), respectively. The synthesis of FSRs was carried out similarly to the synthesis of the previously described MSRs. The bulk polymerization with further cross-linking was conducted by mixing *bis*-D<sub>4</sub> (5 wt.%; 0.19 g, 0.25 mmol for FSR25; 0.41 g, 0.55 mmol for FSR50) with D<sub>4</sub> (1.75 g, 5.90 mmol), Fc<sub>4</sub>D<sub>4</sub> (2.15 g, 1.97 mmol for FSR25; 6.42 g, 5.90 mmol for FSR50), and APDMST (0.06 g, 0.29 mmol for FSR25; 0.13 g, 0.63 mmol for FSR50) in a round-bottom flask under argon at 100 °C. Afterwards, the reaction mixture was sealed and stirred at 100 °C for ≈3 h. The formed viscous gel was poured into a PTFE mold with a surface area of 160 mm length × 40 mm width and dried at 100 °C for 24 h. The obtained films of FSRs with a thickness of ≈1 mm were peeled off the PTFE mold and cut out to obtain shapes according to the requirements of further experiments.

## 3. Results and Discussion

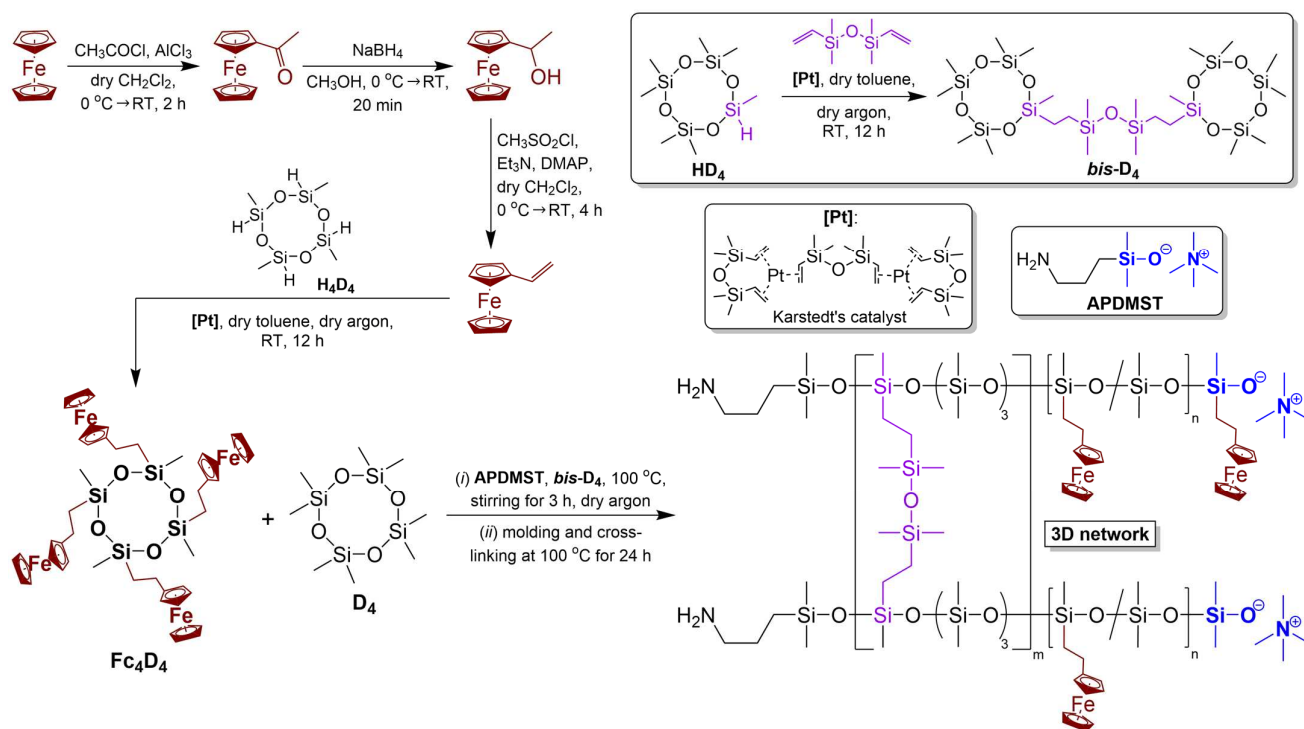
### 3.1. Preparation and Structure of Ferrocenyl-Containing Silicone Rubbers

Figure 1 presents a synthetic scheme for FSRs, which includes (i) the synthesis of a bicyclic cross-linking agent with a Si–O–Si linker between the tetrasiloxane cycles (*bis*-D<sub>4</sub>) by catalytic hydrosilylation; (ii) the catalytic hydrosilylation of vinylferrocene with 1,3,5,7-tetramethylcyclotetrasiloxane (H<sub>4</sub>D<sub>4</sub>) to obtain a tetraferrocenyl-substituted cyclic siloxane (Fc<sub>4</sub>D<sub>4</sub>) [72]; and (iii) ROAP of D<sub>4</sub>, Fc<sub>4</sub>D<sub>4</sub>, and *bis*-D<sub>4</sub> in order to prepare target FSRs. At the first stage, both reactions of catalytic hydrosilylation were conducted in the presence of Karstedt's catalyst, and their completion was confirmed by <sup>1</sup>H, <sup>13</sup>C, and <sup>29</sup>Si NMR spectroscopy (Figures S1 and S2, Supplementary Material). In the HRMS spectra of *bis*-D<sub>4</sub> and Fc<sub>4</sub>D<sub>4</sub> monomers (Figures S3 and S4), molecular ions (*m*/*z*) were found with their characteristic isotopic distribution. For the next stage, APDMST initiator was synthesized and used instead of TMAH for ROAP since it had proven itself to be one of the most effective, according to the reference [67]. The following cross-linking ROAP reaction of Fc<sub>4</sub>D<sub>4</sub> with *bis*-D<sub>4</sub> was performed with the addition of D<sub>4</sub> to enlarge the number of anionic centers and facilitate “pre-copolymerization” in the presence of initiator APDMST, leading to the formation of FSRs films. It should be noted that initially immiscible D<sub>4</sub> and Fc<sub>4</sub>D<sub>4</sub> dissolve into each other during ROAP. The molar ratio of D<sub>4</sub> and Fc<sub>4</sub>D<sub>4</sub> was chosen as 3:1 and 1:1 to prepare FSRs with ferrocenyl-substituted unit content of 25 and 50 mol.% (FSR25 and FSR50, respectively), as in the case of previously studied non-self-healable ferrocenyl-containing silicone rubbers [9,54–57]. The introduction of a smaller amount of ferrocenyl moieties than 25 mol.% is impractical due to the low ferrocene content, a significant decrease in electrical conductivity (down to a typical dielectric, 1·10<sup>−15</sup> S·cm<sup>−1</sup>), and a decline in redox properties [9,54–57]. However, the excess of Fc<sub>4</sub>D<sub>4</sub> (ferrocenyl unit content >50 mol.%) caused a hindrance to cross-linking and led to obtain a liquid material.

By means of an example of FSR25, the obtained 3D polymer networks were characterized by SSNMR spectroscopy (<sup>1</sup>H, <sup>13</sup>C, and <sup>29</sup>Si) and compared with the initial liquid Fc<sub>4</sub>D<sub>4</sub> and *bis*-D<sub>4</sub> monomers (Figure S5). Thus, the <sup>1</sup>H SSNMR spectrum included intensive broad signals of dimethylsiloxane and (2-ferrocenylethyl)methylsiloxane units ( $\delta \approx 0.22, 0.98, 1.50, 1.88, 2.52, \text{ and } 4.15$  ppm) as well as small broad signals from cross-links formed from *bis*-D<sub>4</sub> ( $\delta \approx 0.08$  and 0.58 ppm). In the <sup>13</sup>C SSNMR spectrum, only signals of dimethylsiloxane and (2-ferrocenylethyl)methylsiloxane units are indicated ( $\delta \approx 1.9, 22.9, 25.7, 69.2, \text{ and } 93.9$  ppm) without cross-links.

The most notable difference between monomers and the 3D polymer network is established by <sup>29</sup>Si SSNMR. This spectrum shows an intensive signal of Si nuclei, which is connected with dimethylsiloxane chains ( $\delta \approx -22.3$  ppm [73]), and a new signal of Si atoms from (2-ferrocenylethyl)methylsiloxane units of a polymer backbone ( $\delta \approx -23.0$ ), which are different from that of Fc<sub>4</sub>D<sub>4</sub> (the small signals of the remaining monomer are  $\delta \approx -19.7$  and  $-20.4$  ppm). According to the reference [74], increasing the size of the substituted and non-substituted cyclic oligosiloxanes in rows D<sub>3</sub>–D<sub>4</sub>–D<sub>5</sub> as well as their polymerization

causes changes in  $^{29}\text{Si}$  chemical shifts to more negative values. This bibliographic fact confirms the polymerization of  $\text{Fc}_4\text{D}_4$ . In addition, a small signal of Si–O–Si cross-links ( $\delta \approx 7.9$  ppm) is detected. Hence, the results of the  $^{29}\text{Si}$  SSNMR are fully consistent with the fact that most of the  $\text{Fc}_4\text{D}_4$  cycles copolymerized with  $\text{D}_4$  and *bis*- $\text{D}_4$ , which acted as a cross-linker during ROAP.



**Figure 1.** General synthetic scheme of FSRs. DMAP—4-dimethylaminopyridine.

The iron and ferrocene content in the obtained FSRs was estimated using EDX spectroscopy. According to the obtained data in Table 1, the practical iron content in the FSRs slightly exceeds the theoretically calculated one. For the FSR50, the practical iron content in comparison with the theoretical one turns out to be greater than that of the FSR25. This fact indicates that the ROAP of the initial cyclic oligosiloxanes is more difficult with an increase in the molar fraction of  $\text{Fc}_4\text{D}_4$ . As a result, a part of  $\text{D}_4$  did not enter ROAP by evaporating within the cross-linking process.

**Table 1.** Iron and ferrocene content in the FSRs.

Silicone Rubber	Fe Content, wt.%		Ferrocene Content, wt.%	
	Theoretically Calculated	Determined by EDX	Theoretically Calculated	Determined by EDX
FSR25	10.9	$11.7 \pm 0.1$	36.1	$38.7 \pm 0.5$
FSR50	15.3	$16.5 \pm 0.2$	50.8	$54.6 \pm 0.7$

### 3.2. Cross-Linking Degree and Tensile Properties

The films of FSRs swell in organic solvents (toluene,  $\text{CHCl}_3$ , etc.) but do not dissolve in them, thereby making it possible to estimate the cross-linking degree of FSRs by the swelling measurements. The experiments were carried out in a Soxhlet extractor using toluene as a good solvent at toluene's boiling point ( $110^\circ\text{C}$ ). The cross-linking degree and the average molecular weight of the segments between cross-links ( $M_c$ ) were calculated for each rubber according to the Flory–Rehner equation [68]. The swelling data of FSRs correlate with each other depending on ferrocene content. The  $\omega_{\text{sol}}$  parameter rises, while

the  $\nu$  value declines with an increase in the ferrocene content in FSRs (Table 2). When  $\text{Fc}_4\text{D}_4$  content increases with  $\text{D}_4$  fraction declining, the cross-linking reaction of the FSRs proceeds slower, which is expressed in a decrease in the cross-linking degree in the FSR25–FSR50 series. Thus, a higher content of ferrocenyl groups in FSRs and, therefore, a smaller number of cross-links formed from *bis*- $\text{D}_4$  lead to a lower cross-linking degree ( $M_c$  rises from 60,000 to 85,200 in the FSR25–FSR50 series).

**Table 2.** Swelling and tensile properties of the FSRs and PDMSbis $\text{D}_4$ -0.5%.

Silicone Rubber	$\rho_p$ , $\text{g}\cdot\text{mL}^{-1}$	Swelling Properties			Tensile Properties			
		$s$ , %	$\omega_{sol}$ , %	$\nu$	$M_c$	$\sigma$ , MPa	$\epsilon$ , %	$\epsilon_{residual}$ , %
FSR25	$1.08 \pm 0.03$	$550 \pm 50$	$51 \pm 9$	$0.11 \pm 0.03$	60,000	$0.08 \pm 0.02$	$215 \pm 25$	100
FSR50	$1.11 \pm 0.05$	$420 \pm 40$	$66 \pm 11$	$0.10 \pm 0.03$	85,200	$0.10 \pm 0.01$	$200 \pm 20$	200
PDMSbis $\text{D}_4$ -0.5%	$1.00 \pm 0.03$	$450 \pm 40$	$43 \pm 7$	$0.15 \pm 0.04$	32,300	$0.10 \pm 0.02$	$1600 \pm 200$	— <sup>1</sup>

<sup>1</sup> The parameters could not be determined.

FSRs are characterized by a relatively narrow range of elongation at break ( $\epsilon$ ) and tensile strength ( $\sigma$ ), which change antibatically with increasing ferrocene content in the FSR25–FSR50 series (Figure 2a, Table 2). Despite the lower cross-linking degree, the FSR50 ( $\sigma = 0.10$  MPa) is slightly stronger than the FSR25 ( $\sigma = 0.08$  MPa). These results are incompatible with the swelling properties described above and the calculated cross-linking degrees but can be explained by the influence of the content of volumetric ferrocenyl groups in the FSRs. The higher the content of the ferrocenyl side groups, the more rigid the siloxane backbone. Therefore, the increase in ferrocene content leads to higher  $\sigma$  values.

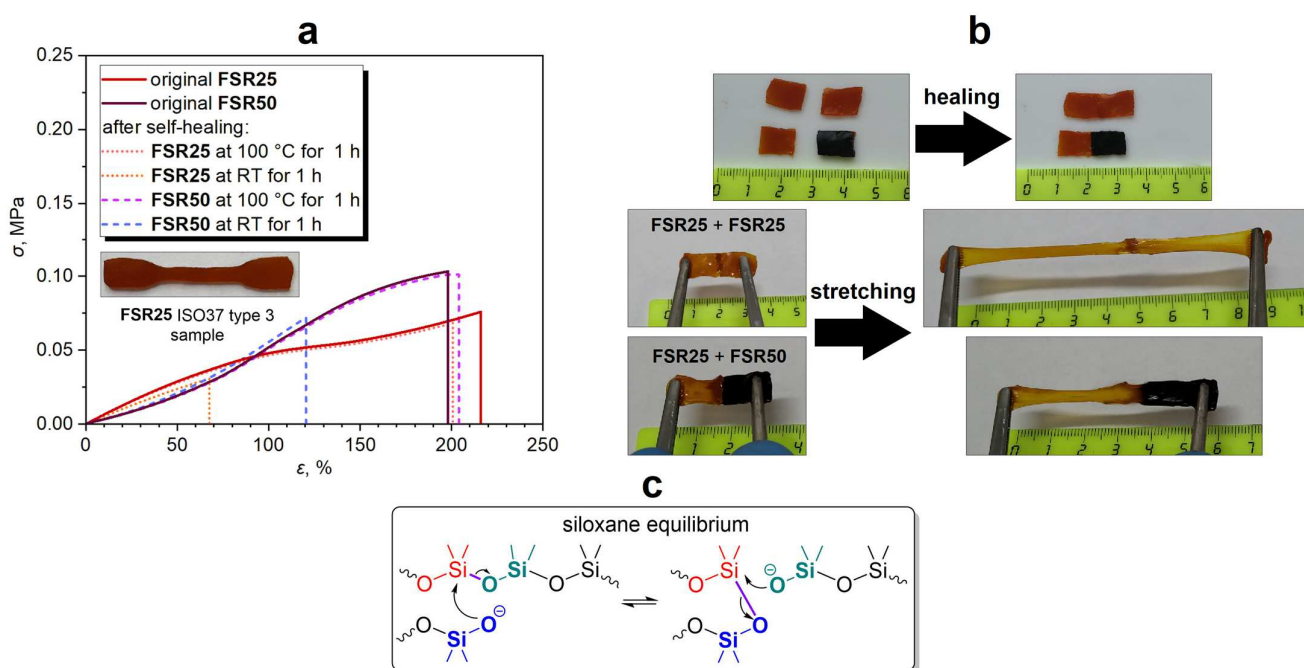


**Figure 2.** Stress–strain curves of the original and healed FSRs at a stretching speed of  $40 \text{ mm}\cdot\text{min}^{-1}$  (a), demonstration of self-healing properties for FSRs (b), and scheme of siloxane equilibrium (c).

On the other hand, the optimal concentration of the cross-linking agent for FSRs was 5 wt.%, whereas it was 0.5 wt.% for model self-healing silicone rubbers (MSRs), which can be explained by the ferrocenyl groups influence on decreasing the cross-linking degree ( $M_c$  is up to 32,300 and 85,200 for MSRs and FSRs, respectively) (Table 2 and Table S1). It should be noted that MSRs could not be successfully prepared with a concentration of *bis*- $\text{D}_4$  similar to that of FSRs (5 wt.%) due to fast cross-linking with extreme bubbling.

Thus,  $\sigma$  and  $\epsilon$  values for MSRs with 0.5–1.0 wt.% of *bis*-D<sub>4</sub> are at levels of >0.10 MPa and >200% that are higher than in the case of FSRs (Table 2 and Table S1, and Figure S6).

### 3.3. Self-Healing Properties

According to references [60–65], the self-healing ability of FSRs and MSRs can be rationalized by siloxane equilibrium in the dynamic 3D polymer network, as shown in Figure 2b,c. To estimate the self-healing efficiency ( $\eta$ ), the polymer strips were cut into two pieces and joined together to allow self-healing, and afterwards, tension tests of the original and healed strips were performed to measure the  $\eta$  parameter. Thus, the obtained FSRs exhibit self-healing ability at room and/or elevated temperatures (100 °C). The rate of self-healing increases with increasing temperature. Thus, in the cases of FSR25 and FSR50, the self-healing efficiency achieves 40 and 71% after being healed for 1 h at RT (Table 3, Figure 2a and Figure S7). On the contrary, the  $\eta$  parameter reaches 89 and 98% after being healed for 1 h at 100 °C for FSR25 and FSR50, respectively (Table 3, Figure 2a and Figure S7). As a result, FSR50 has a better ability to self-heal than FSR25 since it has a lower cross-linking degree, as previously described (Table 2). However, the MSR with a higher cross-linking degree ( $M_c = 32,300$ , 0.5 wt.% of *bis*-D<sub>4</sub>) demonstrated greater self-healing efficiencies at RT and 100 °C than those of FSRs (Table 3 and Table S2, and Figure S8). This fact could be explained by higher chain mobility in MSR networks due to the lack of volumetric ferrocenyl side groups in their structure.

**Table 3.** Self-healing properties of the FSRs compared to MSRs.

Silicone Rubber	Healing Temperature, °C	Healing Time	$\eta$ , %
FSR25	RT	1 h	40
		5 min	55
	100	15 min	66
		30 min	82
		1 h	89
FSR50	RT	1 h	71
	100	1 h	98
PDMSbisD <sub>4</sub> -0.5%	RT	24 h	90
	100	15 min	100

### 3.4. Electrophysical and Electrochemical Properties

The specific electrical conductivity of FSRs was estimated by using broadband impedance spectroscopy in the solid state under the influence of an applied high-frequency current from 10<sup>1</sup> to 10<sup>6</sup> Hz. For studying conductivity, the FSRs were directly cross-linked on an electrode. The MSR with the lowest cross-linking degree (PDMSbisD<sub>4</sub>-0.5%) was tested as a reference dielectric sample. Comparison of the specific bulk conductivity of FSRs with that of PDMSbisD<sub>4</sub>-0.5% at RT clearly shows that conductivity rises from 1·10<sup>-15</sup> to 3·10<sup>-10</sup> S·cm<sup>-1</sup> at 100 Hz in the MSR–FSR25–FSR50 series (approximately 10<sup>5</sup> times; Figure 3a). This electrophysical behavior of the FSRs confirms the materials have an electron-hopping or tunneling nature [54,75–77].

By means of an example of FSR25, the redox properties of FSRs were determined by CV. To obtain a working electrode, the drop casting method of the FSR25 onto a GC electrode was used by direct copolymerization reaction of Fc<sub>4</sub>D<sub>4</sub>, D<sub>4</sub>, and *bis*-D<sub>4</sub> in the required ratio: the ROAP was carried out in a flask at 100 °C for 1 h, followed by cross-linking on the electrode surface at 90 °C for 2 h. A 0.1 M LiClO<sub>4</sub> solution in a mixture of H<sub>2</sub>O–CH<sub>3</sub>CN (4:1, V/V) was used as an electrolyte. The CV measurements were conducted at various potential sweep rates from 10 to 1000 mV·s<sup>-1</sup> (Figure 3b) utilizing the GC electrode modified by FSR25. Thus, only one pair of oxidation/reduction peaks corresponding to

the  $\text{Fc}/\text{Fc}^+$  transformation at redox potential  $E^0 \approx 0.43 \text{ V}$  is observed (Figure 3b). The electrochemical behavior is similar to that of previously obtained FSRs [57] and indicates a semi-infinite diffusion control at scan rates since there is a square root dependence between the peak current and the potential scan rate both in the case of the anodic and cathodic current peaks (Figure 3b).

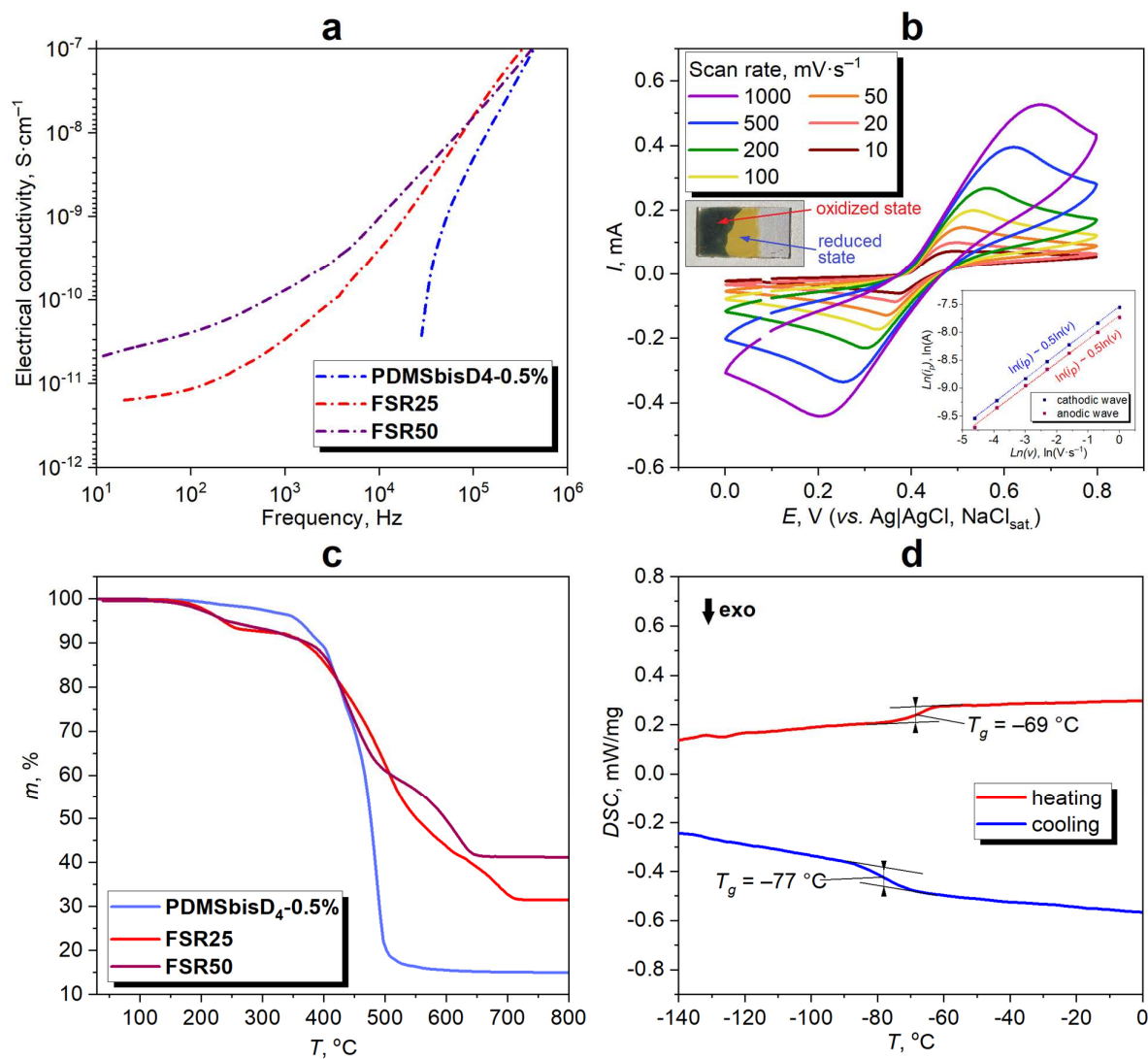


**Figure 3.** The frequency dependence of electrical conductivity of FSRs and model PDMSbisD<sub>4</sub>-0.5% at RT (a), CV curves of FSR25 film deposited on a GC electrode recorded at various potential sweep rates in 0.1 M LiClO<sub>4</sub> H<sub>2</sub>O–CH<sub>3</sub>CN (4:1, V/V) solution with dependence of peak current  $i_p$  on the potential sweep rate  $v$  in bilogarithmic coordinates and demonstration of EC (FSR25 deposited on ITO glass shows EC as in the case of the previously reported FSRs [57]) (b), TG curves of FSRs and model PDMSbisD<sub>4</sub>-0.5% from 25 to 800 °C (c), and DSC curves for FSR25 from –140 to 0 °C (d).

As a result, the FSRs have redox activity combined with a low specific electrical conductivity of up to approximately  $10^{-10}$ – $10^{-11} \text{ S}\cdot\text{cm}^{-1}$  (at 100 Hz), which is an appropriate level for antistatic protective materials [34,35,54,57].

### 3.5. Thermal Properties

The thermal properties of FSR25, FSR50, and model PDMSbisD<sub>4</sub>-0.5% were established by using TG in an aerial atmosphere (Figure 3c). The temperature of gradual weight loss for all FSRs is independent of ferrocene content and is ca. 200 °C, which is lower than in the case of PDMSbisD<sub>4</sub>-0.5% (thermally stable up to ca. 350 °C). After thermal treatment, the

residual masses of FSR50, FSR25, and PDMSbisD<sub>4</sub>-0.5% are 41, 31, and 15%, respectively. Therefore, the residual mass decreases at 800 °C in the FSR50–FSR25–MSR series with a decline in the iron content (ferrocenyl groups transform into Fe<sub>3</sub>O<sub>4</sub> during oxidation) in the same sequence. The mechanism of thermal degradation is described in detail in the references [57,78,79].

Using the DSC technique, it was found that the glass transition temperature ( $T_g$ ) for FSR25 was between  $-77$  and  $-69$  °C (Figure 3d). As distinguished from PDMSbisD<sub>4</sub>-0.5% with typical  $T_g = -128$  °C [6,7] (Figure S9), peaks corresponding to crystallization and melting processes were not observed on the DSC curves. It should be concluded that the FSR25 has an amorphous 3D polymer network due to the atactic configuration of ferrocenyl-containing moieties in the siloxane chains.

#### 4. Conclusions

A method was developed for obtaining simultaneously redox-active and self-healing silicone materials based on ferrocenyl-containing polysiloxanes with a dynamic 3D polymer network based on siloxane equilibrium. The FSRs were synthesized with different ferrocenyl unit content (25 and 50 mol.%) by anionic copolymerization of cyclic octamethylcyclotetrasiloxane (D<sub>4</sub>), cyclic tetraferrocenyl-substituted 1,3,5,7-tetramethyltetrasiloxane (Fc<sub>4</sub>D<sub>4</sub>), and bicyclic oligosiloxane cross-linking agent (*bis*-D<sub>4</sub>).

The optimal concentration of the cross-linking agent for FSRs is 5 wt.%. The FSR with a ferrocenyl-substituted unit content of 25 mol% (FSR25) is the most optimal in terms of cross-linking degree ( $M_c = 60,000$ ), which is higher than that of FSR50 ( $M_c = 85,200$ ), and mechanical hysteresis (the residual elongation after break of ca. 100%). The FSR25 and FSR50 possess tensile strengths of 0.08 and 0.10 MPa and elongation at break of ca. 215 and 200%, which change oppositely with the cross-linking degree. Thus, the average molecular weight of the segment between cross-links ( $M_c$ ) rises from 60,000 to 85,200 with the increase in tensile strength in the FSR25–FSR50 series that could be explained by higher siloxane chain stiffness due to higher ferrocenyl group content in FSR50.

The obtained FSRs exhibit self-healing ability at RT and/or elevated temperatures (100 °C) by siloxane equilibrium in the dynamic 3D polymer network [60–65]. The self-healing efficiency achieves 89 and 98% after being healed for 1 h at 100 °C for FSR25 and FSR50, respectively, which is similar to that of the previously reported non-autonomous self-healing silicone rubbers including bipyridinic polymer-metal complexes (with Fe<sup>2+</sup>, Eu<sup>3+</sup>, Tb<sup>3+</sup>, Tm<sup>3+</sup>, etc.,  $\eta$  is up to 90% after being healed at 100 °C for 2 days) [2,71] and siloxane equilibrium-based silicones (healing at RT and 70–90 °C for several minutes to 24 h) [62–65].

As distinguished from the well-known self-healing siloxane equilibrium-based silicones without ferrocenyl fragments [62–65], the FSRs possess not only self-healing properties but also redox activity and antistatic properties. The FSRs have redox activity combined with a low specific electrical conductivity of up to approximately  $10^{-10}$ – $10^{-11}$  S·cm<sup>-1</sup> (at 100 Hz), which is an appropriate level for antistatic materials [54,57] and ca. 10–100 times higher than that of the reported self-healing polymer-metal complexes [31,69,70,80]. The conductivity and redox properties result from the reduction-oxidation of ferrocenyl groups (Fc/Fc<sup>+</sup> transformations at  $E^0$  ca. 0.43 V). As in the case of previously published FSRs [54,57], the low conductivity of the ferrocenyl-containing polymers exhibits electron tunneling behavior, making the FSRs useful as electrostatic discharge materials.

In this regard, the flexibility, stretchability, self-healing, and good film-forming ability of FSRs can be important for creating coatings based on them. The conductivity at the level of antistatic materials and the redox activity of FSRs make them useful for fabricating electrostatic dissipative coatings. The proposed approach is relevant for the creation of new functional polymer materials that will expand the use of silicone materials in flexible, self-healing, and antistatic protective coatings.

**Supplementary Materials:** The following supplementary material can be downloaded at: <https://www.mdpi.com/article/10.3390/coatings13071282/s1>, Figure S1:  $^1\text{H}$  (a),  $^{13}\text{C}$  (b), and  $^{29}\text{Si}$  NMR spectra (c) of *bis*-D<sub>4</sub> and its isomers (d); Figure S2:  $^1\text{H}$  (a),  $^{13}\text{C}$  (b), and  $^{29}\text{Si}$  NMR spectra (c) of Fc<sub>4</sub>D<sub>4</sub> and its general structure (d); Figure S3: HRMS spectrum of *bis*-D<sub>4</sub>; Figure S4: HRMS spectrum of Fc<sub>4</sub>D<sub>4</sub>; Figure S5:  $^1\text{H}$  (a),  $^{13}\text{C}$  (b), and  $^{29}\text{Si}$  SSNMR spectra (c) of FSR25 and the fragment of its 3D polymer network (d); Figure S6: Stress–strain curves of the MSRs at a stretching speed of 40 mm·min<sup>−1</sup>; Figure S7: Stress–strain curves of the original and healed FSR25 (a) and FSR50 (b) at a stretching speed of 40 mm·min<sup>−1</sup>; Figure S8: Stress–strain curves of the original and healed MSRs: PDMSbisD<sub>4</sub>-0.5% (a) and PDMSbisD<sub>4</sub>-0.75% (b) at a stretching speed of 40 mm·min<sup>−1</sup>; Figure S9: DSC curves for PDMSbisD<sub>4</sub>-0.5% from −140 to 0 °C; Table S1: Swelling and tensile properties of the MSRs; Table S2: Self-healing properties of the MSRs.

**Author Contributions:** Methodology, investigation, writing—original draft preparation, and visualization, A.A.R.; validation, formal analysis, writing—original draft preparation, data curation, visualization, project administration, funding, and acquisition, K.V.D.; methodology and investigation, E.K.P.; validation, resources, writing—review and editing, and supervision, R.M.I. All authors have read and agreed to the published version of the manuscript.

**Funding:** This research was funded by the Russian Science Foundation (Grant Number 23-23-00103).

**Institutional Review Board Statement:** Not applicable.

**Informed Consent Statement:** Not applicable.

**Data Availability Statement:** All data are reported within the present article.

**Acknowledgments:** The physicochemical measurements were performed at the Magnetic Resonance Research Centre, Chemical Analysis and Materials Research Centre, the Centre for Innovative Technologies of Composite Nanomaterials, and the Cryogenic Department (which are parts of St. Petersburg University).

**Conflicts of Interest:** The authors declare no conflict of interest.

## References

1. *Polymer Coatings: Technologies and Applications*, 1st ed.; Rangappa, S.M.; Parameswaranpillai, J.; Siengchin, S. (Eds.) CRC Press: Boca Raton, FL, USA, 2020; ISBN 978-0-429-19922-6.
2. Deriabin, K.V.; Filippova, S.S.; Islamova, R.M. Self-Healing Silicone Materials: Looking Back and Moving Forward. *Biomimetics* **2023**, *8*, 286. [\[CrossRef\]](#)
3. Cheng, M.; Fu, Q.; Tan, B.; Ma, Y.; Fang, L.; Lu, C.; Xu, Z. Build a Bridge from Polymeric Structure Design to Engineering Application of Self-Healing Coatings: A Review. *Prog. Org. Coat.* **2022**, *167*, 106790. [\[CrossRef\]](#)
4. Udoh, I.I.; Shi, H.; Daniel, E.F.; Li, J.; Gu, S.; Liu, F.; Han, E.-H. Active Anticorrosion and Self-Healing Coatings: A Review with Focus on Multi-Action Smart Coating Strategies. *J. Mater. Sci. Technol.* **2022**, *116*, 224–237. [\[CrossRef\]](#)
5. Cazacu, M.; Dascalu, M.; Stiubianu, G.-T.; Bele, A.; Tugui, C.; Racles, C. From Passive to Emerging Smart Silicones. *Rev. Chem. Eng.* **2022**. [\[CrossRef\]](#)
6. Yilgör, E.; Yilgör, I. Silicone Containing Copolymers: Synthesis, Properties and Applications. *Prog. Polym. Sci.* **2014**, *39*, 1165–1195. [\[CrossRef\]](#)
7. Mark, J.E.; Schaefer, D.W.; Lin, G. *The Polysiloxanes*; Oxford University Press: Oxford, UK, 2015; ISBN 978-0-19-518173-9.
8. Moretto, H.-H.; Schulze, M.; Wagner, G. Silicones. In *Ullmann's Encyclopedia of Industrial Chemistry*; Wiley-VCH Verlag GmbH & Co. KGaA: Weinheim, Germany, 2000; p. a24\_057. ISBN 978-3-527-30673-2.
9. Deriabin, K.V.; Islamova, R.M. Ferrocenyl-Containing Oligosiloxanes and Polysiloxanes: Synthesis, Properties, and Application. *Polym. Sci. Ser. C* **2022**, *64*, 95–109. [\[CrossRef\]](#)
10. Miroshnichenko, A.S.; Neplokh, V.; Mukhin, I.S.; Islamova, R.M. Silicone Materials for Flexible Optoelectronic Devices. *Materials* **2022**, *15*, 8731. [\[CrossRef\]](#)
11. Guo, R.; Zhou, L.; Lin, J.; Chen, G.; Zhou, Z.; Li, Q. Self-Healing, High-Strength, and Antimicrobial Polysiloxane Based on Amino Acid Hydrogen Bond. *Macromol. Rapid Commun.* **2023**, *44*, 2200657. [\[CrossRef\]](#)
12. Sun, J.; Liu, C.; Duan, J.; Liu, J.; Dong, X.; Zhang, Y.; Wang, N.; Wang, J.; Hou, B. Facile Fabrication of Self-Healing Silicone-Based Poly(Urea-Thiourea)/Tannic Acid Composite for Anti-Biofouling. *J. Mater. Sci. Technol.* **2022**, *124*, 1–13. [\[CrossRef\]](#)
13. Liu, J.; Zheng, N.; Li, Z.; Liu, Z.; Wang, G.; Gui, L.; Lin, J. Fast Self-Healing and Antifouling Polyurethane/Fluorinated Polysiloxane-Microcapsules-Silica Composite Material. *Adv. Compos. Hybrid Mater.* **2022**, *5*, 1899–1909. [\[CrossRef\]](#)
14. Wang, P.; Wang, B.; He, B.; Liu, S.; Ye, Q.; Zhou, F.; Liu, W. In Situ Generation of Zwitterionic-Functionalized Liquid Metal-Based Polydimethylsiloxane Antifouling Coatings with Self-Healing Ability. *Prog. Org. Coat.* **2023**, *181*, 107604. [\[CrossRef\]](#)

15. Sun, J.; Duan, J.; Liu, X.; Dong, X.; Zhang, Y.; Liu, C.; Hou, B. Environmentally Benign Smart Self-Healing Silicone-Based Coating with Dual Antifouling and Anti-Corrosion Properties. *Appl. Mater. Today* **2022**, *28*, 101551. [[CrossRef](#)]
16. Filippova, S.S.; Deriabin, K.V.; Perevyazko, I.; Shamova, O.V.; Orlov, D.S.; Islamova, R.M. Metal- and Peroxide-Free Silicone Rubbers with Antibacterial Properties Obtained at Room Temperature. *ACS Appl. Polym. Mater.* **2023**, *5*, 5286–5296. [[CrossRef](#)]
17. Wang, G.; Li, A.; Zhao, W.; Xu, Z.; Ma, Y.; Zhang, F.; Zhang, Y.; Zhou, J.; He, Q. A Review on Fabrication Methods and Research Progress of Superhydrophobic Silicone Rubber Materials. *Adv. Mater. Interfaces* **2021**, *8*, 2001460. [[CrossRef](#)]
18. Liang, H.; Kuang, Q.; Hu, C.; Chen, J.; Lu, X.; Huang, Y.; Yan, H. Construction of Durable Superhydrophobic and Anti-Icing Coatings via Incorporating Boroxine Cross-Linked Silicone Elastomers with Good Self-Healability. *Soft Matter* **2022**, *18*, 8238–8250. [[CrossRef](#)] [[PubMed](#)]
19. Lai, P.; Yuan, Y.; Huang, Y.; Bai, H.; Zhou, Z.; Tang, C.; Wen, J.; Liu, L. Preparation of Robust, Room-Temperature Self-Healable and Recyclable Polysiloxanes Based on Hierarchical Hard Domains. *Adv. Eng. Mater.* **2023**, *25*, 2300129. [[CrossRef](#)]
20. Allahdini, A.; Jafari, R.; Momen, G. Room-Temperature Microcapsule-Based Self-Healing and Fluorine-Free Superhydrophobic Coating. *Mater. Today Commun.* **2023**, *34*, 105087. [[CrossRef](#)]
21. Li, R.; Tian, S.; Tian, Y.; Wang, J.; Xu, S.; Yang, K.; Yang, J.; Zhang, L. An Extreme-Environment-Resistant Self-Healing Anti-Icing Coating. *Small* **2023**, *19*, 2206075. [[CrossRef](#)]
22. Zhang, B.; Zhang, P.; Zhang, H.; Yan, C.; Zheng, Z.; Wu, B.; Yu, Y. A Transparent, Highly Stretchable, Autonomous Self-Healing Poly(Dimethyl Siloxane) Elastomer. *Macromol. Rapid Commun.* **2017**, *38*, 1700110. [[CrossRef](#)]
23. Lee, J.M.; Park, J.; Ko, J.; Shin, Y.; Shin, D.; Shim, W.; Lee, J.H.; Kappl, M.; Lee, J.; Wooh, S. Autonomous Self-Healable Scratch-Free Bilayer Anti-Corrosion Film. *Appl. Surf. Sci.* **2023**, *631*, 157484. [[CrossRef](#)]
24. Boumezgane, O.; Suriano, R.; Fedel, M.; Tonelli, C.; Deflorian, F.; Turri, S. Self-Healing Epoxy Coatings with Microencapsulated Ionic PDMS Oligomers for Corrosion Protection Based on Supramolecular Acid-Base Interactions. *Prog. Org. Coat.* **2022**, *162*, 106558. [[CrossRef](#)]
25. Mo, P.; Hu, Z.; Mo, Z.; Chen, X.; Yu, J.; Selim, M.S.; Sun, R.; Xu, J.; Zeng, X.; Hao, Z. Fast Self-Healing and Self-Cleaning Anticorrosion Coating Based on Dynamic Reversible Imine and Multiple Hydrogen Bonds. *ACS Appl. Polym. Mater.* **2022**, *4*, 4709–4718. [[CrossRef](#)]
26. Wang, T.; Wang, W.; Feng, H.; Sun, T.; Ma, C.; Cao, L.; Qin, X.; Lei, Y.; Piao, J.; Feng, C.; et al. Photothermal Nanofiller-Based Polydimethylsiloxane Anticorrosion Coating with Multiple Cyclic Self-Healing and Long-Term Self-Healing Performance. *Chem. Eng. J.* **2022**, *446*, 137077. [[CrossRef](#)]
27. Ji, X.; Wang, W.; Zhao, X.; Wang, L.; Ma, F.; Wang, Y.; Duan, J.; Hou, B. Poly(Dimethyl Siloxane) Anti-Corrosion Coating with Wide PH-Responsive and Self-Healing Performance Based on Core-shell Nanofiber Containers. *J. Mater. Sci. Technol.* **2022**, *101*, 128–145. [[CrossRef](#)]
28. Feng, Z.; Guo, J.; Cao, X.; Feng, G.; Chen, Z.; Zhang, X.-H. A Thermo-Reversible Furfuryl Poly(Thioether)-*b*-Polysiloxane-*b*-Furfuryl Poly(Thioether) Triblock Copolymer as a Promising Material for High Dielectric Applications. *Polym. Chem.* **2022**, *13*, 1376–1386. [[CrossRef](#)]
29. Li, M.; Cao, B.; Shang, R.; Mei, H.; Wang, L. Synthesis of Poly(Urea-Formaldehyde) Microcapsules for the Self-Healing System of Silicone Rubber Insulating Material. *J. Appl. Polym. Sci.* **2022**, *139*, e53021. [[CrossRef](#)]
30. Sun, W.; Luo, J.; Zhang, L.; Chen, Y.; Li, P.; Zheng, Y.; Cheng, Y. Insulating Silicones Based on Dynamic Hindered Urea Bonds with High Dielectric Healability and Recyclability. *ACS Appl. Polym. Mater.* **2021**, *3*, 5622–5631. [[CrossRef](#)]
31. Rao, Y.-L.; Chortos, A.; Pfaltner, R.; Lissel, F.; Chiu, Y.-C.; Feig, V.; Xu, J.; Kurosawa, T.; Gu, X.; Wang, C.; et al. Stretchable Self-Healing Polymeric Dielectrics Cross-Linked through Metal-Ligand Coordination. *J. Am. Chem. Soc.* **2016**, *138*, 6020–6027. [[CrossRef](#)]
32. Madsen, F.B.; Yu, L.; Skov, A.L. Self-Healing, High-Permittivity Silicone Dielectric Elastomer. *ACS Macro Lett.* **2016**, *5*, 1196–1200. [[CrossRef](#)]
33. Deriabin, K.V.; Dziuba, M.A.; Rashevskii, A.A.; Kolesnikov, I.E.; Korzhov, A.V.; Sharov, V.A.; Vorobyev, A.; Vereshchagin, A.A.; Chernukha, A.S.; Tian, J.; et al. Nickel(II)-Polysiloxane “Sandwiches” as Electrical Breakdown Protective Materials. *ACS Appl. Polym. Mater.* **2023**, *5*, 892–898. [[CrossRef](#)]
34. Pionteck, J.; Wypych, G. *Handbook of Antistatics*, 2nd ed.; ChemTec Publishing: Toronto, ON, Canada, 2016; ISBN 978-1-895198-95-9.
35. *Paint and Coating Testing Manual: 15th. Edition of the Gardner-Sward Handbook*; Koleske, J.V. (Ed.) ASTM International: West Conshohocken, PA, USA, 2012; ISBN 978-0-8031-7017-9.
36. Pritchard, G. *Plastics Additives: A Rapra Market Report*; Rapra Technology Limited: Shawbury, UK, 2005; ISBN 1-85957-499-8.
37. Soltani, R.; Katbab, A.A. The Role of Interfacial Compatibilizer in Controlling the Electrical Conductivity and Piezoresistive Behavior of the Nanocomposites Based on RTV Silicone Rubber/Graphite Nanosheets. *Sens. Actuators A: Phys.* **2010**, *163*, 213–219. [[CrossRef](#)]
38. Hirasawa, S.; Uchiyama, N.; Tojo, T.; Uyama, T.; Nose, H.; Igarashi, T.; Kanzaki, Z. Cathode Ray Tube with Conductive Silicon Adhesive. US Patent 5757117A; filed 16 August 1996, and issued 26 May 1998,
39. Yao, S.; Zhu, Y. Nanomaterial-Enabled Stretchable Conductors: Strategies, Materials and Devices. *Adv. Mater.* **2015**, *27*, 1480–1511. [[CrossRef](#)]
40. Chen, D.; Pei, Q. Electronic Muscles and Skins: A Review of Soft Sensors and Actuators. *Chem. Rev.* **2017**, *117*, 11239–11268. [[CrossRef](#)]

41. Barshutina, M.N.; Kirichenko, S.O.; Wodolajski, V.A.; Musienko, P.E. Mechanisms of Electrical Conductivity in CNT/Silicone Composites Designed for Neural Interfacing. *Mater. Lett.* **2019**, *236*, 183–186. [[CrossRef](#)]
42. Wang, L.; Chen, Y.; Lin, L.; Wang, H.; Huang, X.; Xue, H.; Gao, J. Highly Stretchable, Anti-Corrosive and Wearable Strain Sensors Based on the PDMS/CNTs Decorated Elastomer Nanofiber Composite. *Chem. Eng. J.* **2019**, *362*, 89–98. [[CrossRef](#)]
43. Montazerian, H.; Dalili, A.; Milani, A.S.; Hoorfar, M. Piezoresistive Sensing in Chopped Carbon Fiber Embedded PDMS Yarns. *Compos. Part B Eng.* **2019**, *164*, 648–658. [[CrossRef](#)]
44. Bezkosty, P.; Długoń, E.; Sowa, M.; Nizioł, J.; Jeleń, P.; Marchewka, J.; Błażewicz, M.; Sitarz, M. Corrosion Resistance and Electrical Conductivity of Hybrid Coatings Obtained from Polysiloxane and Carbon Nanotubes by Electrophoretic Co-Deposition. *IJMS* **2022**, *23*, 2897. [[CrossRef](#)]
45. Beigbeder, J.; Demont, P.; Nabarra, P.; Remaury, S.; Lacabanne, C. Electrical Characterization of Conducting Nanoparticles-Polysiloxane Composites for a Space Durable Coating. In Proceedings of the 2008 13th International Symposium on Electrets, Tokyo, Japan, 15–17 September 2008; p. C214.
46. Hidden, G.; Boudou, L.; Martinez-Vega, J.; Remaury, S.; Nabarra, P. Development of Nanoparticle-Polysiloxane Composites for Spacecraft Applications. *Polym. Eng. Sci.* **2006**, *46*, 1079–1084. [[CrossRef](#)]
47. Smoukov, S.K.; Wang, T.; Farajollahi, M.; Choi, Y.S.; Lin, I.-T.; Marshall, J.E.; Thompson, N.M.; Kar-Narayan, S.; Madden, J.D.W. Electroactive Polymers for Sensing. *Interface Focus* **2016**, *6*, 20160026. [[CrossRef](#)]
48. Xu, F.; Zhang, M.; Cui, Y.; Bao, D.; Peng, J.; Gao, Y.; Lin, D.; Geng, H.; Zhu, Y.; Wang, H. A Novel Polymer Composite Coating with High Thermal Conductivity and Unique Anti-Corrosion Performance. *Chem. Eng. J.* **2022**, *439*, 135660. [[CrossRef](#)]
49. Vörös, J.; Courtine, G.; Larmagnac, A.; Musienko, P. PDMS-Based Stretchable Multi-Electrode and Chemotrode Array for Epidural and Subdural Neuronal Recording, Electrical Stimulation and Drug Delivery. WIPO (PCT) Patent WO2011157714A1; filed 14 June 2011, and issued 22 December 2011,
50. Fujiki, H.; Matsubayashi, S.; Kanto, K.; Suzuki, T. Curable Antistatic Organopolysiloxane Composition and Antistatic Silicone Film. WIPO (PCT) Patent WO2014125826; filed 14 February 2014, and issued 21 August 2014,
51. Kaur, G.; Adhikari, R.; Cass, P.; Bown, M.; Gunatillake, P. Electrically Conductive Polymers and Composites for Biomedical Applications. *RSC Adv.* **2015**, *5*, 37553–37567. [[CrossRef](#)]
52. Orton, J.W. *The Story of Semiconductors*; Oxford University Press: Oxford, UK, 2008; ISBN 978-0-19-955910-7.
53. Schiller, M. PVC Additives. In *PVC Additives*; Carl Hanser Verlag GmbH & Co. KG: München, Germany, 2015; pp. I–XVI.
54. Deriabin, K.V.; Lobanovskaia, E.K.; Kirichenko, S.O.; Barshutina, M.N.; Musienko, P.E.; Islamova, R.M. Synthesis of Ferrocenyl-containing Silicone Rubbers via Platinum-catalyzed Si–H Self-cross-linking. *Appl. Organomet. Chem.* **2020**, *34*, e5300. [[CrossRef](#)]
55. Neplokh, V.; Kochetkov, F.M.; Deriabin, K.V.; Fedorov, V.V.; Bolshakov, A.D.; Eliseev, I.E.; Mikhailovskii, V.Y.; Ilatovskii, D.A.; Krasnikov, D.V.; Tchernycheva, M.; et al. Modified Silicone Rubber for Fabrication and Contacting of Flexible Suspended Membranes of N-/p-GaP Nanowires with a Single-Walled Carbon Nanotube Transparent Contact. *J. Mater. Chem. C* **2020**, *8*, 3764–3772. [[CrossRef](#)]
56. Deriabin, K.V.; Kirichenko, S.O.; Lopachev, A.V.; Sysoev, Y.; Musienko, P.E.; Islamova, R.M. Ferrocenyl-Containing Silicone Nanocomposites as Materials for Neuronal Interfaces. *Compos. Part B Eng.* **2022**, *236*, 109838. [[CrossRef](#)]
57. Deriabin, K.V.; Vereshchagin, A.A.; Kirichenko, S.O.; Rashevskii, A.A.; Levin, O.V.; Islamova, R.M. Self-Cross-Linkable Ferrocenyl-Containing Polysiloxanes as Flexible Electrochromic Materials. *Mater. Today Chem.* **2023**, *29*, 101399. [[CrossRef](#)]
58. *Ferrocenes: Homogeneous Catalysis, Organic Synthesis, Materials Science*, 1st ed.; Togni, A.; Hayashi, T. (Eds.) Wiley-VCH Verlag GmbH & Co. KGaA: Weinheim, Germany, 1995; ISBN 978-3-527-29048-2.
59. Islamova, R.M. Iron Compounds in Controlled Radical Polymerization: Ferrocenes, (Clathro)Chelates, and Porphyrins. *Russ. J. Gen. Chem.* **2016**, *86*, 125–143. [[CrossRef](#)]
60. Osthoff, R.C.; Bueche, A.M.; Grubb, W.T. Chemical Stress-Relaxation of Polydimethylsiloxane Elastomers <sup>1</sup>. *J. Am. Chem. Soc.* **1954**, *76*, 4659–4663. [[CrossRef](#)]
61. Kantor, S.W.; Grubb, W.T.; Osthoff, R.C. The Mechanism of the Acid- and Base-Catalyzed Equilibration of Siloxanes. *J. Am. Chem. Soc.* **1954**, *76*, 5190–5197. [[CrossRef](#)]
62. Zheng, P.; McCarthy, T.J. A Surprise from 1954: Siloxane Equilibration Is a Simple, Robust, and Obvious Polymer Self-Healing Mechanism. *J. Am. Chem. Soc.* **2012**, *134*, 2024–2027. [[CrossRef](#)]
63. Schmolke, W.; Perner, N.; Seiffert, S. Dynamically Cross-Linked Polydimethylsiloxane Networks with Ambient-Temperature Self-Healing. *Macromolecules* **2015**, *48*, 8781–8788. [[CrossRef](#)]
64. Moskalenko, Y.E.; Bagutski, V.; Thiele, C.M. Chemically Synthesized and Cross-Linked PDMS as Versatile Alignment Medium for Organic Compounds. *Chem. Commun.* **2017**, *53*, 95–98. [[CrossRef](#)] [[PubMed](#)]
65. Von Szczepanski, J.; Danner, P.M.; Opris, D.M. Self-Healable, Self-Repairable, and Recyclable Electrically Responsive Artificial Muscles. *Adv. Sci.* **2022**, *9*, 2202153. [[CrossRef](#)] [[PubMed](#)]
66. Plevová, K.; Mudráková, B.; Šebesta, R. A Practical Three-Step Synthesis of Vinylferrocene. *Synthesis* **2018**, *50*, 760–763. [[CrossRef](#)]
67. Hoffman, J.J.; Leir, C.M. Tetramethylammonium 3-Aminopropyl Dimethylsilylanolate—Aminopropyl Dimethylsilylanolate—A New Catalyst for the Synthesis of High Purity, High Molecular Weight  $\alpha,\omega$ -Bis(Aminopropyl) Polydimethylsiloxanes. *Polym. Int.* **1991**, *24*, 131–138. [[CrossRef](#)]
68. Sperling, L.H. *Introduction to Physical Polymer Science*, 4th ed.; Wiley: Hoboken, NJ, USA, 2005; ISBN 978-0-471-70606-9.

69. Deriabin, K.V.; Ignatova, N.A.; Kirichenko, S.O.; Novikov, A.S.; Islamova, R.M. Nickel(II)-Pyridinedicarboxamide-Copolydimethylsiloxane Complexes as Elastic Self-Healing Silicone Materials with Reversible Coordination. *Polymer* **2021**, *212*, 123119. [[CrossRef](#)]
70. Deriabin, K.V.; Ignatova, N.A.; Kirichenko, S.O.; Novikov, A.S.; Kryukova, M.A.; Kukushkin, V.Y.; Islamova, R.M. Structural Features of Polymer Ligand Environments Dramatically Affect the Mechanical and Room-Temperature Self-Healing Properties of Cobalt(II)-Incorporating Polysiloxanes. *Organometallics* **2021**, *40*, 2750–2760. [[CrossRef](#)]
71. Miroshnichenko, A.S.; Deriabin, K.V.; Baranov, A.I.; Neplokh, V.; Mitin, D.M.; Kolesnikov, I.E.; Dobrynin, M.V.; Parshina, E.K.; Mukhin, I.S.; Islamova, R.M. Lanthanide(III)-Incorporating Polysiloxanes as Materials for Light-Emitting Devices. *ACS Appl. Polym. Mater.* **2022**, *4*, 2683–2690. [[CrossRef](#)]
72. Casado, C.M.; Cuadrado, I.; Moran, M.; Alonso, B.; Lobete, F.; Losada, J. Synthesis of the First Redox-Active Organometallic Polymers Containing Cyclosiloxanes as Frameworks. *Organometallics* **1995**, *14*, 2618–2620. [[CrossRef](#)]
73. Uhlig, F.; Marsmann, H.C. <sup>29</sup>Si NMR Some Practical Aspects. In *Gelest Catalogue (Silicon Compounds: Silanes & Silicones Aufl.)*; Gelest, Inc.: Morrisville, PA, USA, 2003; pp. 208–222.
74. Kendrick, T.C.; Parbhoo, B.M.; White, J.W. Polymerization of Cyclosiloxanes. In *Comprehensive Polymer Science and Supplements*; Pergamon Press: Oxford, UK, 1989; pp. 459–523. ISBN 978-0-08-096701-1.
75. Blauch, D.N.; Saveant, J.M. Dynamics of Electron Hopping in Assemblies of Redox Centers. Percolation and Diffusion. *J. Am. Chem. Soc.* **1992**, *114*, 3323–3332. [[CrossRef](#)]
76. Gan, L.; Sangeeth, C.S.; Yuan, L.; Jańczewski, D.; Song, J.; Nijhuis, C.A. Tuning Charge Transport across Junctions of Ferrocene-Containing Polymer Brushes on ITO by Controlling the Brush Thickness and the Tether Lengths. *Eur. Polym. J.* **2017**, *97*, 282–291. [[CrossRef](#)]
77. Pietschnig, R. Polymers with Pendant Ferrocenes. *Chem. Soc. Rev.* **2016**, *45*, 5216–5231. [[CrossRef](#)] [[PubMed](#)]
78. Delebecq, E.; Hamdani-Devarenes, S.; Raeke, J.; Cuesta, J.-M.L.; Ganachaud, F. High Residue Contents Indebted by Platinum and Silica Synergistic Action during the Pyrolysis of Silicone Formulations. *ACS Appl. Mater. Interfaces* **2011**, *3*, 869–880. [[CrossRef](#)] [[PubMed](#)]
79. Hamdani, S.; Longuet, C.; Perrin, D.; Lopez-cuesta, J.-M.; Ganachaud, F. Flame Retardancy of Silicone-Based Materials. *Polym. Degrad. Stab.* **2009**, *94*, 465–495. [[CrossRef](#)]
80. Li, C.-H.; Wang, C.; Keplinger, C.; Zuo, J.-L.; Jin, L.; Sun, Y.; Zheng, P.; Cao, Y.; Lissel, F.; Linder, C.; et al. A highly stretchable autonomous self-healing elastomer. *Nat. Chem.* **2016**, *8*, 618–624. [[CrossRef](#)] [[PubMed](#)]

**Disclaimer/Publisher’s Note:** The statements, opinions and data contained in all publications are solely those of the individual author(s) and contributor(s) and not of MDPI and/or the editor(s). MDPI and/or the editor(s) disclaim responsibility for any injury to people or property resulting from any ideas, methods, instructions or products referred to in the content.